ESSENTIALLY NON-OSCILLATORY SHOCK CAPTURING METHODS APPLIED TO TURBULENCE AMPLIFICATION IN SHOCK WAVE CALCULATIONS

Stanley Osher[1]
Department of Mathematics
University of California
Los Angeles, CA 90024

Chi-Wang Shu[2]
Division of Applied Mathematics
Brown University
Providence, RI 02912

ENO (essentially non-oscillatory) schemes can provide uniformly high order accuracy right up to discontinuities while keeping sharp, essentially non-oscillatory shock transitions. Recently we obtained an efficient implementation of ENO schemes based on fluxes and TVD Runge-Kutta time discretizations. The resulting code is very simple to program for multi-dimensions. ENO schemes are especially suitable for computing problems with BOTH discontinuities AND fine structures in smooth regions, such as shock interaction with turbulence, for which results for one dimensional and two dimensional Euler equations are presented. We observe much better resolution by using third order ENO schemes than by using second order TVD schemes for such problems.

Efficient Implementation of ENO Schemes

The solutions to systems of hyperbolic conservation laws of the type

$$\mathbf{u}_t + \sum_{i=1}^{d} \mathbf{f}_i(\mathbf{u})_{x_i} = 0 \quad (\text{or } = g(\mathbf{u}, \mathbf{x}, t), \text{ a forcing term}) \tag{1.1a}$$

$$\mathbf{u}(\mathbf{x}, 0) = \mathbf{u}^0(\mathbf{x}) \tag{1.1b}$$

where $\mathbf{u} = u_1, \ldots, u_m)^T$, $\mathbf{x} = (x^1, \ldots, x^d)$, and for real $\xi = (\xi_1, \ldots, \xi_d)$, the combination $\sum_{i=1}^{d} \xi_i \frac{\partial \mathbf{f}_i}{\partial \mathbf{u}}$ is assumed to have m real eigenvalues and a complete set of eigenvectors, may develop discontinuities (shocks, contact discontinuities, etc.) regardless of the smoothness of the initial condition. Examples of (1.1) include Euler equations of gas dynamics. ENO schemes, originally constructed by Harten, Osher, Engquist and Chakravarthy [1-4], use a local adaptive

[1]Research supported by NSF Grant No. DMS85-03294, DARPA Grant in the ACMP Program, ONR Grant N00014-86-K-0691, NASA Langley Grant NAG-1-270
[2]Research supported by NSF Grant No. DMS88-10150

stencil to obtain information automatically from regions of smoothness when the solution develops discontinuities. As a result, approximations using these methods can obtain uniformly high order accuracy right up to discontinuities, while keeping a sharp essentially non-oscillatory shock transition. The original ENO schemes in [1-4] used a cell-average framework which involved a reconstruction procedure to recover accurate point values from cell averages, and a Lax-Wendroff procedure (replacing time derivatives by space derivatives, using the P.D.E.) for the time discretization. This can become a bit complicated for multi-dimensional problems [1]. For ease of implementation we constructed [7, 8] ENO schemes applying the adaptive stencil idea to the numerical fluxes and using a TVD Runge-Kutta type high order time discretization. These ENO schemes skip the reconstruction step and the Lax-Wendroff time discretization procedure, hence the resulting code is simple for multi-space dimensional problems.

Let us describe our scheme first in scalar, one dimensional case ($d = m = 1$ in (1.1)). The scheme, in its method-of-lines form, is

$$\frac{du_j}{dt} = L(u)_j \equiv -\frac{1}{\Delta x}(\hat{f}_{j+\frac{1}{2}} - \hat{f}_{j-\frac{1}{2}}) \tag{1.2}$$

where the numerical flux $\hat{f}_{j+\frac{1}{2}}$ approximates $h(x_{j+\frac{1}{2}})$ to a high order, with $h(x)$ defined by

$$f(u(x)) = \frac{1}{\Delta x}\int_{x-\frac{\Delta x}{2}}^{x+\frac{\Delta x}{2}} h(\xi)d\xi \tag{1.3}$$

We first obtain the primitive function of $h(x)$:

$$H(x) = \int_{-\infty}^{x} h(\xi)d\xi \tag{1.4}$$

at $x_{j+\frac{1}{2}}$ by

$$H(x_{j+\frac{1}{2}}) = \int_{-\infty}^{x_{j+\frac{1}{2}}} h(\xi)d\xi = \sum_{k=-\infty}^{j}\int_{x_{k-\frac{1}{2}}}^{x_{k+\frac{1}{2}}} h(\xi)d\xi = \Delta x \sum_{k=-\infty}^{j} f(u_k), \tag{1.5}$$

then construct polynomials interpolating $\{H_{j+\frac{1}{2}}\}$ in an ENO fashion, i.e. by obtaining a locally "smoothest" stencil starting from one or two points, then adding one point to the stencil at each stage by comparing two divided differences and choosing the one which is smaller in absolute value. $\hat{f}_{j+\frac{1}{2}}$ is then taken as the derivative of this interpolating polynomial evaluated at $x_{j+\frac{1}{2}}$. "Upwinding" is achieved by the initial choice in the stencil-choosing process, and it is also crucial for the evident stability of these methods. We also need an entropy fix in any "expansion shock cell". For details, see [7, 8].

The time discretization of (1.2) is implemented via a class of TVD Runge-Kutta type methods [7]. For example, the third order case is

$$u^{(1)} = u^{(0)} + \Delta t L(u^{(0)}) \tag{1.6a}$$

$$u^{(2)} = \frac{3}{4}u^{(0)} + \frac{1}{4}u^{(1)} + \frac{1}{4}\Delta t L(u^{(1)}) \tag{1.6b}$$

$$u^{(3)} = \frac{1}{3}u^{(0)} + \frac{2}{3}u^{(2)} + \frac{2}{3}\Delta t L(u^{(2)}) \tag{1.6c}$$

$$u^{(0)} = u^n,\ u^{n+1} = u^{(3)} \tag{1.6d}$$

This class of Runge-Kutta methods was shown to have the property that the total variation of the spatial part is not increased during the time discretization under a suitable restriction on $\frac{\Delta t}{\Delta x}$.

For multi-dimensions the right-hand-side of (1.2) is applied to each of the terms $f_i(u)_{x_i}$ in (1.1a), keeping all other variables fixed. The Runge-Kutta methods such as (1.6) can still be applied.

For nonlinear systems, we simply apply the algorithms in each local characteristic field. We take an 1-dimensional system to exemplify this process. Let $A_{j+\frac{1}{2}}$ be some "average" Jacobian at $x_{j+\frac{1}{2}}$. Examples include $A_{j+\frac{1}{2}} = \frac{\partial \mathbf{f}}{\partial \mathbf{u}}\big|_{\mathbf{u}=\frac{1}{2}(\mathbf{u}_j+\mathbf{u}_{j+1})}$ or, in the case of Euler equations of gas dynamics $A_{j+\frac{1}{2}} = \frac{\partial \mathbf{f}}{\partial \mathbf{u}}\big|_{\mathbf{u}=\mathbf{u}^{(\mathrm{Roe})}_{j+\frac{1}{2}}}$ where $\mathbf{u}^{(\mathrm{Roe})}_{j+\frac{1}{2}}$ is the Roe average of $\mathbf{u}_j$ and $\mathbf{u}_{j+1}$ [6]. We then use the eigenvalues of $A_{j+\frac{1}{2}}$, project to the local characteristic fields: and finally apply our scalar algorithms in each of these fields. See [8] for more details.

2. Numerical Tests – Shock Interaction with Turbulence

Example 1. We start with one dimensional Euler equations of gas dynamics for a polytropic gas, i.e. (1.1) with $d = 1$, $m = 3$, and

$$\mathbf{u} = (\rho, M, E)^T, \quad \mathbf{f}(\mathbf{u}) = q\mathbf{u} + (0, P, qP)^T \tag{2.1a}$$

where

$$P = (\gamma - 1)(E - \frac{1}{2}\rho q^2), \quad M = \rho q \tag{2.1b}$$

We use $\gamma = 1.4$, and an initial condition

$$\begin{cases} \rho = 3.857143; & q = 2.629369; \quad P = 10.333333 \quad \text{when } x < -4 \\ \rho = 1 + \varepsilon \sin 5x; & q = 0; \quad P = 1 \qquad\qquad \text{when } x \geq -4 \end{cases} \tag{2.2}$$

If $\varepsilon = 0$, this is a pure Mach = 3 shock moving to the right.

For a detailed linearized analysis see [5]. This linearized analysis, predicts fine structures for the density profile because of the different propagation speeds of entropy and acoustic waves. For

ε small (say $\varepsilon = 0.05$) we observe results close to linearized analysis. For $\varepsilon = 0.2$ we can observe nonlinear effects such as additional small shocks in the density profile.

This is a good test problem because both shocks and fine structures in smooth regions exist. Traditional high order methods will develop oscillations near shocks, and TVD methods, while nonlinearly stable, will lose resolution for the fine structures because of the degeneracy to first order accuracy at smooth critical points.

In Figure 1-4, the solid lines are numerical solutions of third order ENO scheme (henceforth shortened to ENO-3) with 1600 grid points. This can be regarded as a converged solution. From Figure 1, we see that ENO-3 with 400 points almost gives a converged solution, while TVD-2 (a second order MUSCL type TVD scheme) with 800 points just has roughly the same resolution as ENO-3 with 200 points. On the other hand, the improvement of ENO-3 over TVD-2 is not so significant for the velocity and pressure profiles (Figure 2), because they both lack any detailed structure.

To further exemplify the advantage of higher order methods, we increase the spatial order of our ENO scheme and compare density and entropy profiles with 300 grid points using ENO-3, 4, 5, 6. We clearly observe better resolution by going to higher spatial orders (Figure 3). In Figure 3 the time discretization is third order (1.6) with Δt decreased for high spatial orders. When we use higher order time discretizations as well we observe further improvements in resolution (pictures not included).

We finally test the effect of physical viscosities by solving the Navier-Stokes equation, i.e. (1.1)-(2.1) with a right-hand-side

$$(0, \frac{4}{3} \cdot \frac{1}{\mathrm{Re}} q_{xx},\ \frac{1}{\mathrm{Re}} \cdot \frac{2}{3}(q^2)_{xx} + \frac{1}{(\gamma-1) \cdot P_r \cdot \mathrm{Re} \cdot M^2}(\frac{E}{\rho} - \frac{1}{2}q^2)_{xx})^T \tag{2.3}$$

We used $Pr = 1$, $M = 3$ and gradually increased the Reynolds number Re. Clearly we observe (Figure 4) convergence to Euler's result as the physical viscosity goes to zero ($\mathrm{Re} \to \infty$). To verify the theory (rigorously proven by Kreiss) that for wave lengths $> c \cdot \frac{1}{\sqrt{\mathrm{Re}}}$ the problem is viscosity dominated and otherwise essentially inviscid, we re-ran our result with a different frequency for the sine wave. We do observe the correctness of the above theory with $c \approx 3$ in our scaling. The pictures are omitted.

Example 2. Next we come to two dimensional Euler equations, i.e. (1.1) with $d = 2$, $m = 4$, and (we use $\mathbf{f}, \mathbf{g}, x, y$ instead of $\mathbf{f}_1, \mathbf{f}_2, x_1, x_2$):

$$\begin{gathered} \mathbf{u} = (\rho, M_x, M_y, E)^T, \quad \mathbf{f}(\mathbf{u}) = \mathbf{q}_x \mathbf{u} + (0, P, 0, q_x P)^T \\ \mathbf{g}(\mathbf{u}) = q_y \mathbf{u} + (0, 0, P, q_y P)^T \end{gathered} \tag{2.4a}$$

where

$$P = (\gamma - 1)(E - \frac{1}{2}\rho q^2), \quad q^2 = q_x^2 + q_y^2, \quad M_x = \rho q_x, \quad M_y = \rho q_y \tag{2.4b}$$

The test problem we choose is a moving shock interacting with compressible turbulence [9, 10]. At $t = 0$, a Mach 8 shock at $x = -1.0$ is moving into a state with $P_R = 1$, $\rho_R = 1$ and $q_x = -\frac{C_R}{P_R}\sin\theta_r \cos(xk_R\cos\theta_R + yk_R\sin\theta_R)$, $q_y = \frac{C_R}{P_R}\cos\theta_R\cos(xk_R\cos\theta_R + yk_R\sin\theta_R)$ where $k_R = 2\pi, \theta_R = \frac{\pi}{6}$, and $C_R = \sqrt{\frac{\gamma P_R}{\rho_R}}$. We display the results at $t = 0.20$ in Figure 5. Notice that in [9, 10] similar results were obtained using a shock-fitting rather than a shock capturing method. This is actually a two dimensional analogue of Example 1 – a combination of shocks and fine structures in smooth regions. Hence it is again a good test problem for the high order ENO schemes. The successful computation of this example shows that ENO schemes have excellent potential for shock-turbulence computations.

Acknowledgements: We thank David Gottlieb, Ami Harten, Lawrence Sirovich and Thomas Zang for many helpful discussions and suggestions.

References

[1] A. Harten, Preliminary results on the extension of ENO schemes to two-dimensional problems, in Proceedings of the International Conference on Hyperbolic Problems, Saint-Etienne, January 1986.

[2] A. Harten and S. Osher, Uniformly high order accurate non-oscillatory schemes, I, SIAM J. Numer. Anal., 24 (1987), pp. 279-309.

[3] A. Harten, B. Engquist, S. Osher and S. Chakravarthy, Uniformly high order accurate essentially non-oscillatory schemes, III, J. Comput. Phys., 71 (1987), pp. 231-303.

[4] A. Harten, S. Osher, B. Engquist and S. Chakravarthy, Some results on uniformly high order accurate essentially non-oscillatory schemes, J. Appl. Numer. Math., 2 (1986), pp. 347-

[5] J. McKenzie and K. Westphal, Interaction of linear waves with oblique shock waves, Phys. Fluids, 11 (1968), pp. 2350-2362.

[6] P. Roe, Approximate Riemann solvers, parameter vectors, and difference schemes, J. Comput. Phys., 43 (1981), pp. 357-372.

[7] C.-W. Shu and S. Osher, Efficient implementation of essentially non-oscillatory shock capturing schemes, J. Comput. Phys., 77 (1988), pp. 439-471.

[8] C.-W. Shu and S. Osher, Efficient implementation of essentially non-oscillatory shock capturing schemes, II, ICASE Report 88-24, J. Comput. Phys., to appear..

[9] T. Zang, M. Hussaini and D. Bushnell, Numerical computations of turbulence amplification in shock-wave interactions, AIAA J., 22 (1984), pp. 13-21.

[10] T. Zang, D. Kopriva and M. Hussaini, Pseudospectral calculation of shock turbulence interactions, in Proceedings of Numerical Methods Conference, C. Taylor et al, eds., Pineridge Press, Swansea, U.K., (1984), pp. 210-221.

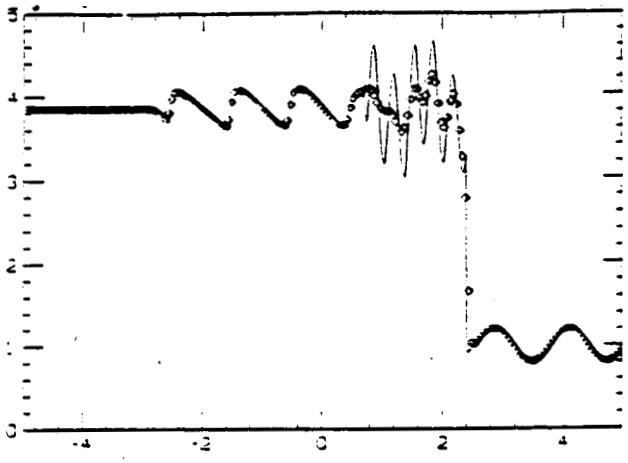

1(a): ENO-3 with 200 points

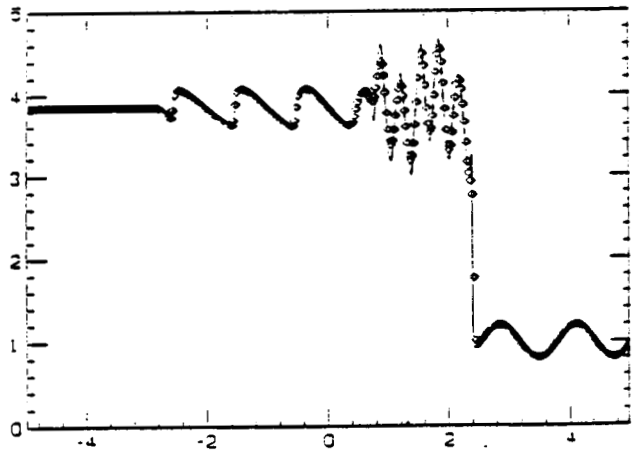

1(b): ENO-3 with 400 points

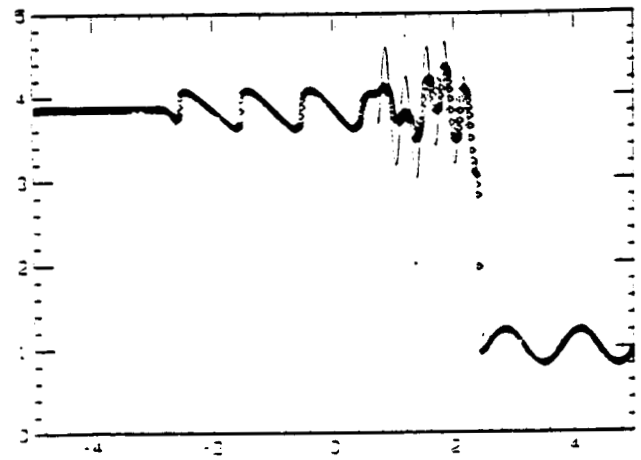

1(c): TVD-2 with 800 points

Figure 1: density

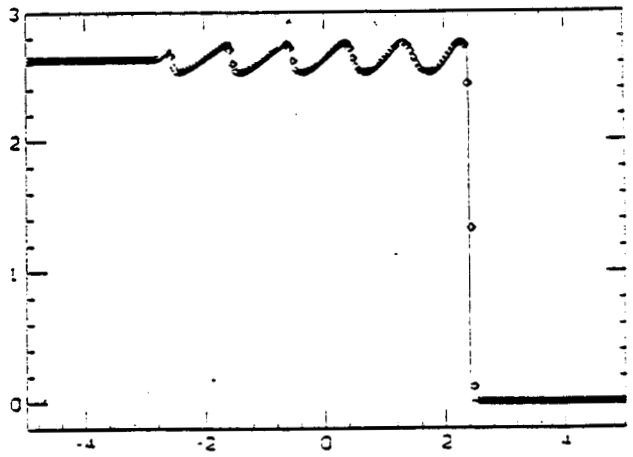

2(a): ENO-3, velocity

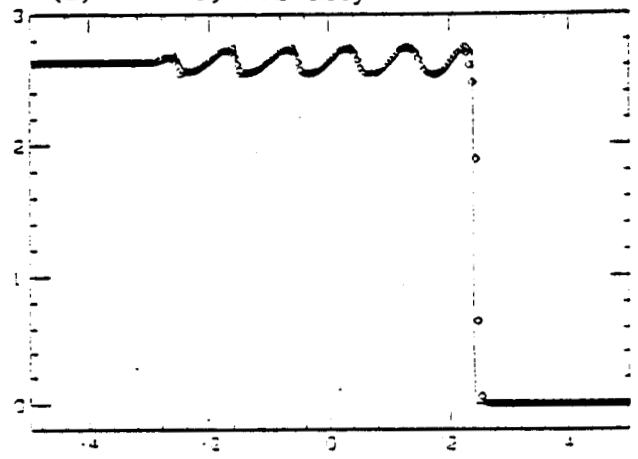

2(b): TVD-2, velocity

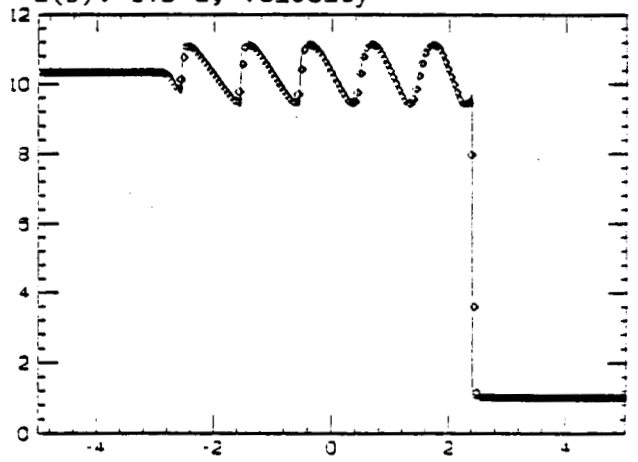

2(c): ENO-3, pressure

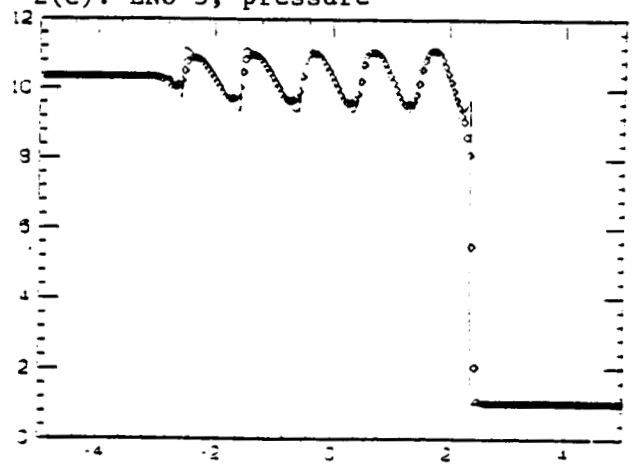

2(d): TVD-2, pressure

Figure 2: 200 points

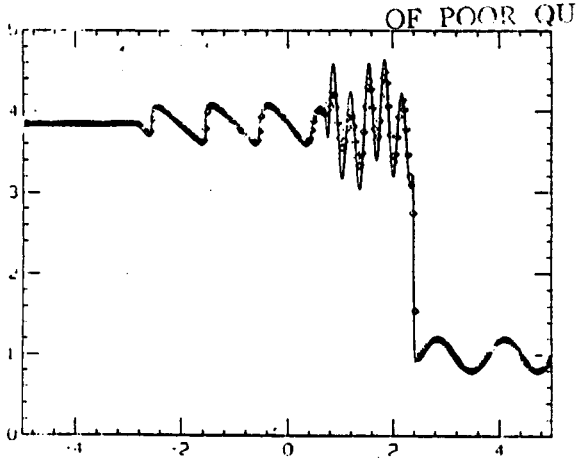

3(a): ENO-3

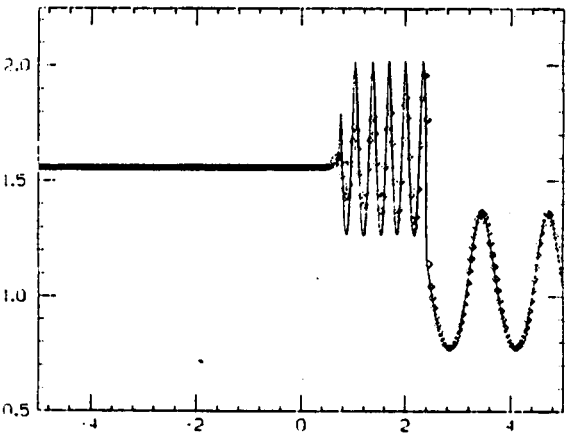

3(e): ENO-3

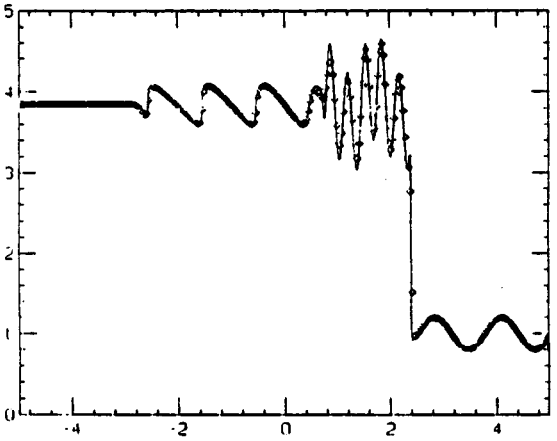

3(b): ENO-4

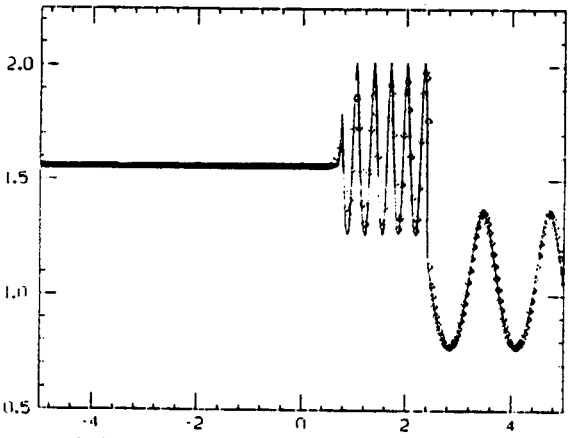

3(f): ENO-4

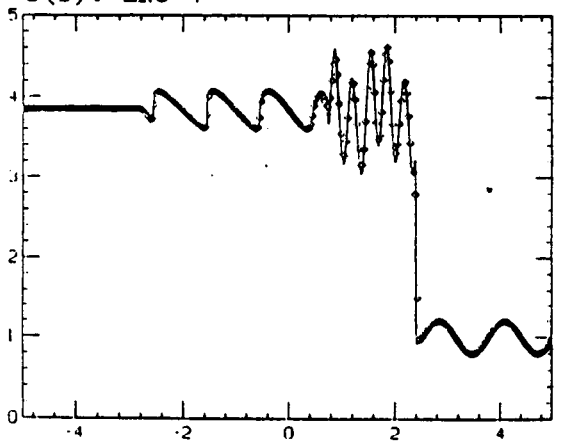

3(c): ENO-5

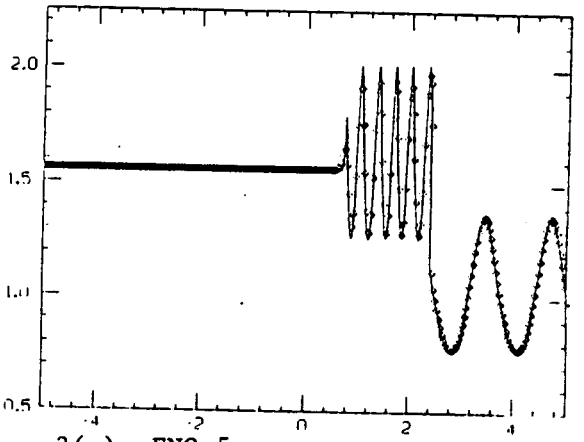

3(g): ENO-5

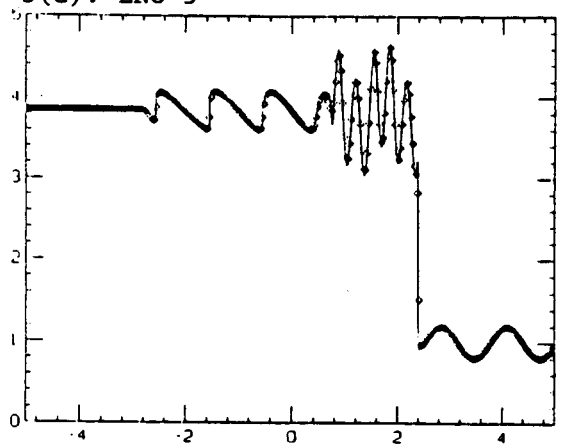

3(d): ENO-6

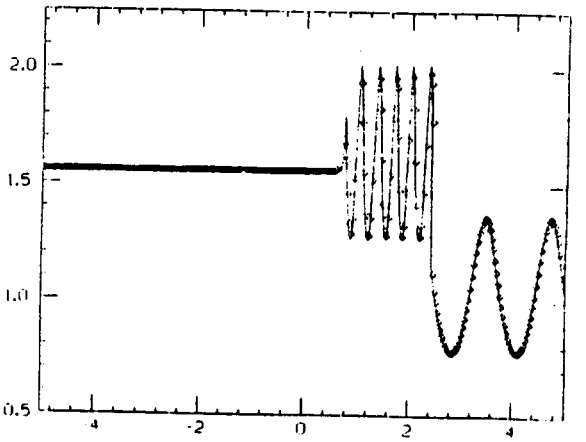

3(h): ENO-6

Figure 3: 300 points, density (left) and entropy (right)

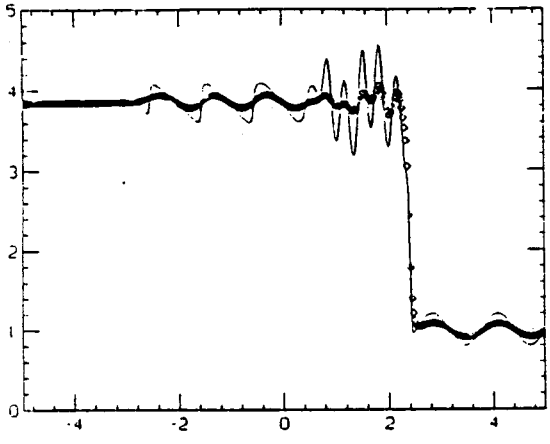

4(a): Re = 10

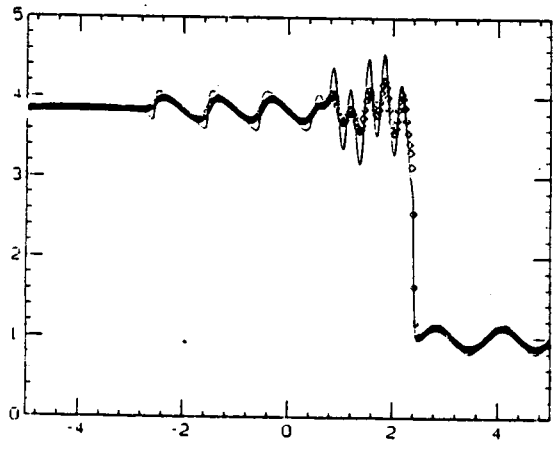

4(b): Re = 20

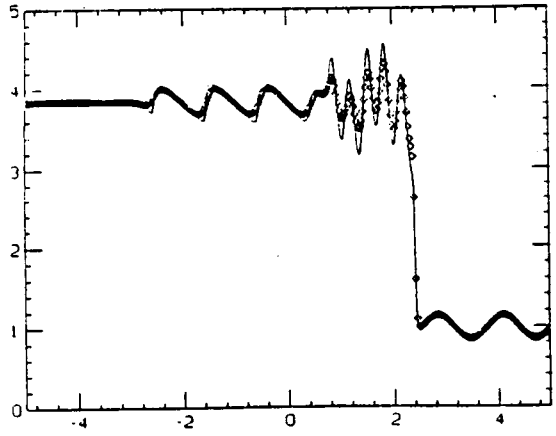

4(c): Re = 30

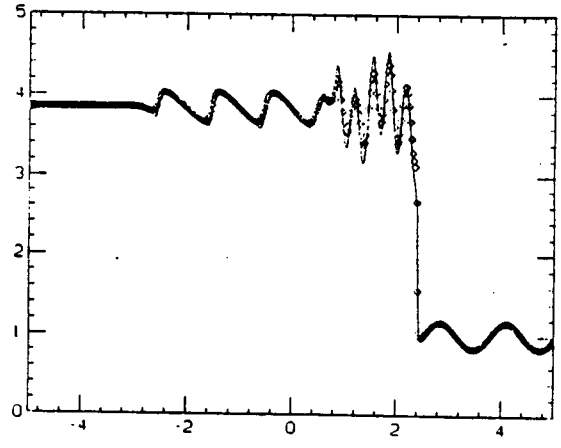

4(d): Re = 50

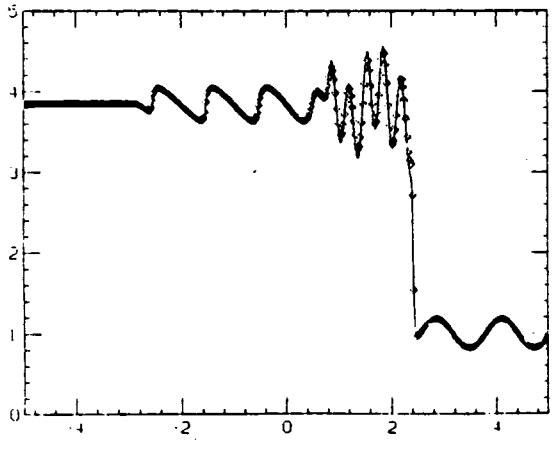

4(e): Re = 100

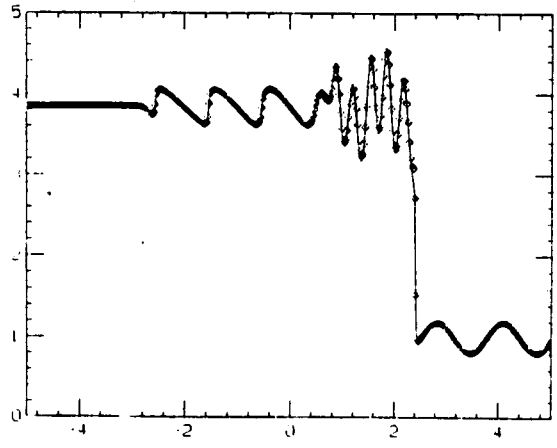

4(f): Re = 200

Figure 4: ENO-3 with 400 points for Navier-Stokes equation.
The solid line is for the solution of Euler's equation.

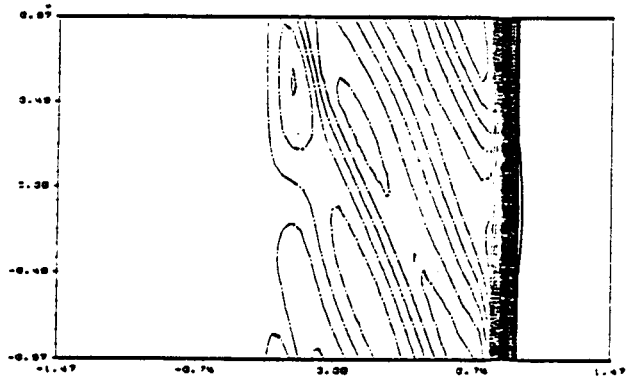

5(a): 60 x 40 points, pressure

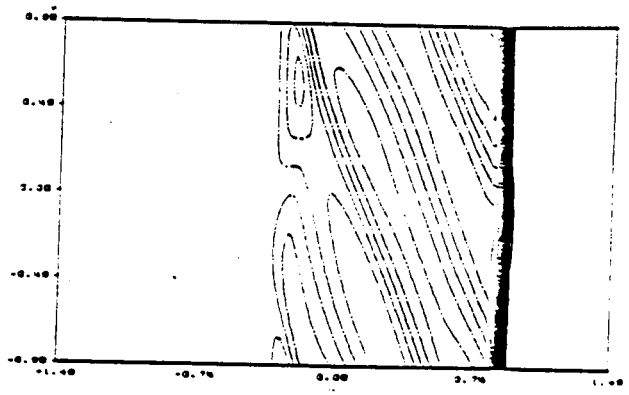

5(d): 120 x 80 points, pressure

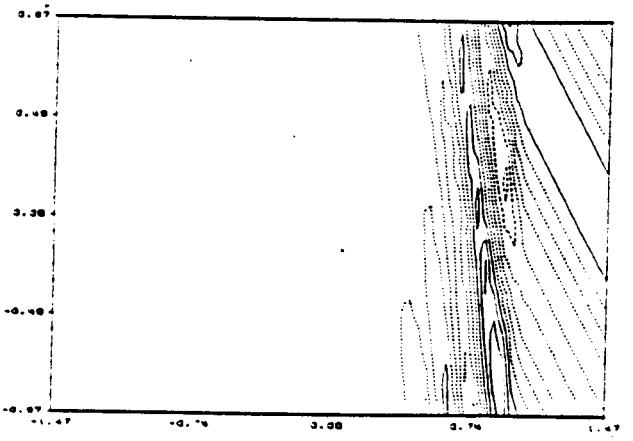

5(b): 60 x 40 points, vorticity

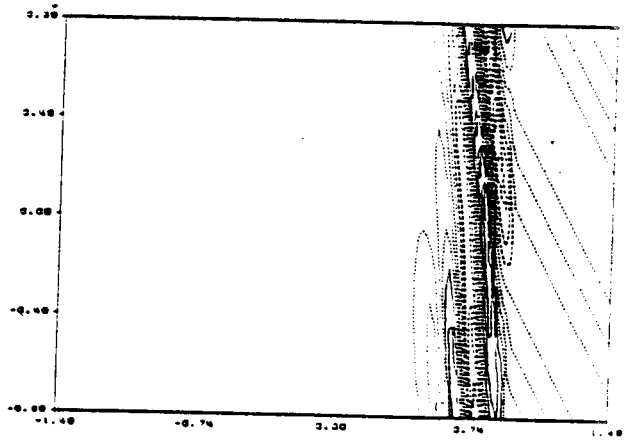

5(e): 120 x 80 points, vorticity

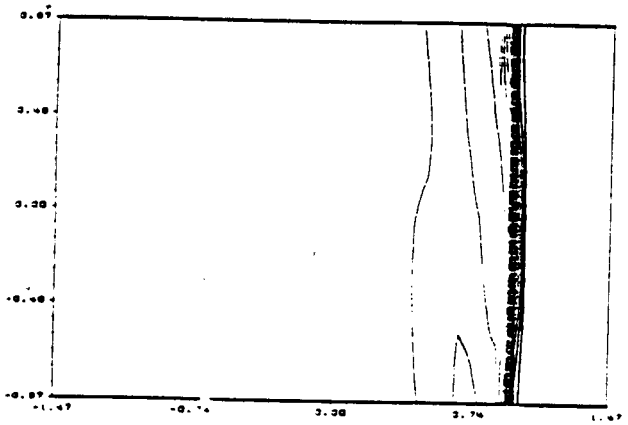

5(c): 60 x 40 points, entropy

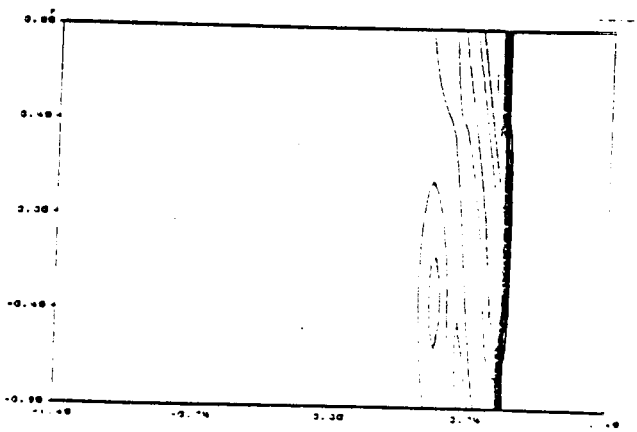

5(f): 120 x 80 points, entropy

Figure 5: ENO-3